Supporting information

Hydrous Nickel Oxyhydroxide Thin Films on Copper Foil as Robust Electrocatalysts for Alkaline Oxygen Evolution

Ankith Shetty[a], Poulami Mukherjee[b], Koichi Higashimine[c], Toshiaki Taniike[b], Vishwanath R. S[a]*, Kalathiparambil Rajendra Pai Sunajadevi[d]*

[a] *Centre for Research in Functional Materials (CRFM), JAIN (Deemed-to-be University), Jain Global Campus, Bengaluru 562112, Karnataka, India.*

[b] *Graduate School of Advanced Science and Technology, Japan Advanced Institute of Science and Technology, 1-1 Asahidai, Nomi, Ishikawa, 923-1292, Japan.*

[c] *Center for Nano Materials and Technology, Japan Advanced Institute of Science and Technology, 1-1 Asahidai, Nomi, Ishikawa, 923-1292, Japan.*

[d] *Department of Chemistry, Christ University, Bengaluru-560029, Karnataka, India.*

***Corresponding authors**

Vishwanath R. S

Email id: vishwanath.rs@jainuniversity.ac.in

Kalathiparambil Rajendra Pai Sunajadevi

Email id: sunajadevi.kr@christuniversity.in

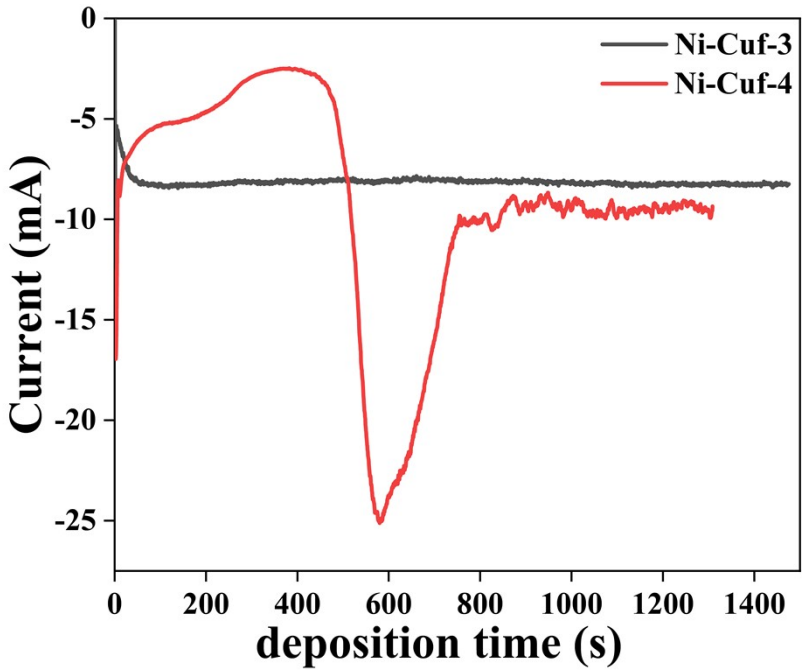

Fig. S1: Potentiostatic bulk electrolysis profiles for Ni deposition onto Cuf at –0.8 V (vs Ag/AgCl) from sulfate baths of initial pH 3 (Ni–Cuf-3) and pH 4 (Ni–Cuf-4).

Fig. S2: Images corresponding to intermediate stages of deposition for Ni-Cuf-3 and Ni-Cuf-4.

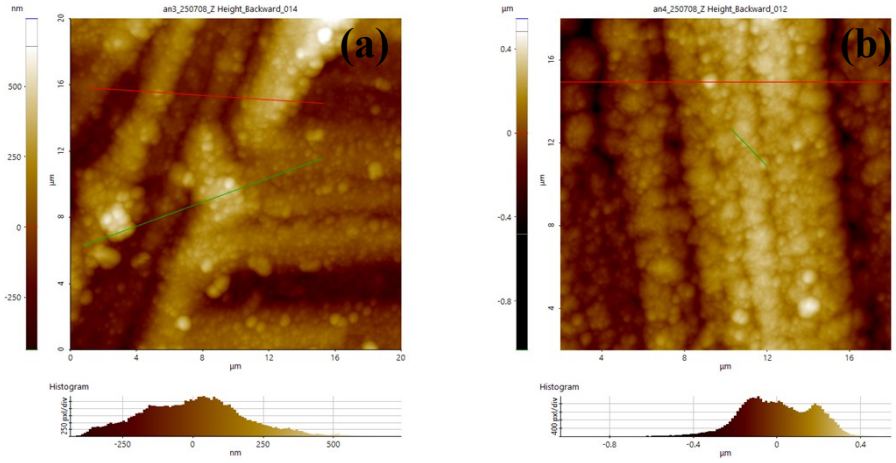

Fig. S3: (a) and (b) AFM-height images with pixel-height distribution of Ni-Cuf-3 and Ni-Cuf-4, respectively.

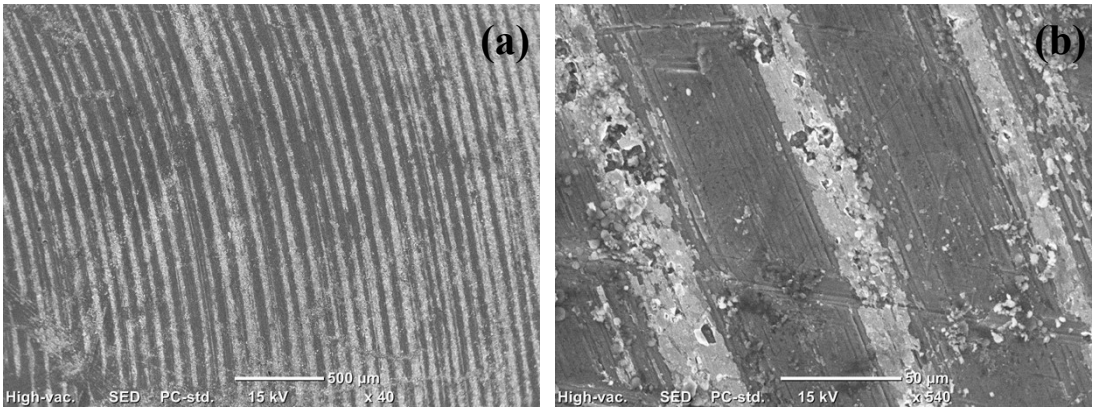

Fig. S4: SEM images of bare Cuf

Table S1: Z-height statistical data of Ni-Cuf-3 and Ni-Cuf-4

Electrodes	Rpv (μm)	Rq (μm)	Ra (μm)	Rz (μm)	Rsk (μm)	Rku (μm)	Length (μm)
Ni-Cuf-3	0.666	0.184	0.158	N/A	0.535	2.055	~ 13 (H)
	0.675	0.182	0.144	N/A	0.200	2.227	~ 16 (H)
	0.124	0.036	0.030	N/A	0.624	2.231	~ 2
	0.340	0.099	0.084	N/A	-0.496	2.176	~ 4
	0.461	0.090	0.063	N/A	-1.397	5.323	~ 9 (V)
	0.585	0.184	0.150	N/A	-1.085	2.686	~3.5
Ni-Cuf-4	0.822	0.180	0.148	N/A	-0.1512	2.472	20 (H)
	0.118	0.031	0.024	N/A	-0.766	2.803	2.5
	0.097	0.029	0.024	N/A	-0.367	0.996	1.6

Texture coefficient (TC) analysis:

The preferred orientation of crystallites in the synthesized samples was evaluated by calculating the texture coefficient (TC) for the most prominent diffraction peaks observed in the X-ray diffraction (XRD) patterns. The TC value for a specific crystallographic plane was determined using the following expression:

$$TC(hkl) = \frac{\frac{I(hkl)}{I0(hkl)}}{\frac{1}{N}\left(\sum_{n=1}^{N}\frac{I(hkl)}{I0(hkl)}\right)}$$

where:

- I(hkl) represents the measured relative intensity of the diffraction peak corresponding to the (hkl) plane,
- I0(hkl) denotes the standard intensity of the same reflection taken from the JCPDS/ICDD reference database (representing a randomly oriented powder sample), and
- N is the total number of diffraction peaks considered in the analysis.

A TC value equal to unity indicates random orientation, while TC > 1 signifies preferred orientation along the corresponding plane. The degree of deviation from unity reflects the extent of texture in the material.

In this work, the TC values were calculated by considering the first *N* major reflections in the XRD pattern, and the obtained results were used to assess the dominant growth direction and crystallographic texture of the samples.

Table S2: TCs of crystallographic planes calculated from GIXRD patterns for Ni-Cuf-3 and Ni-Cuf-4 samples.

Electrode	TC for Ni(111)	TC for Ni(200)	TC for Ni(220)
Ni-Cuf-3	0.79	0.84	1.37
Ni-Cuf-4	1.36	0.62	1.02

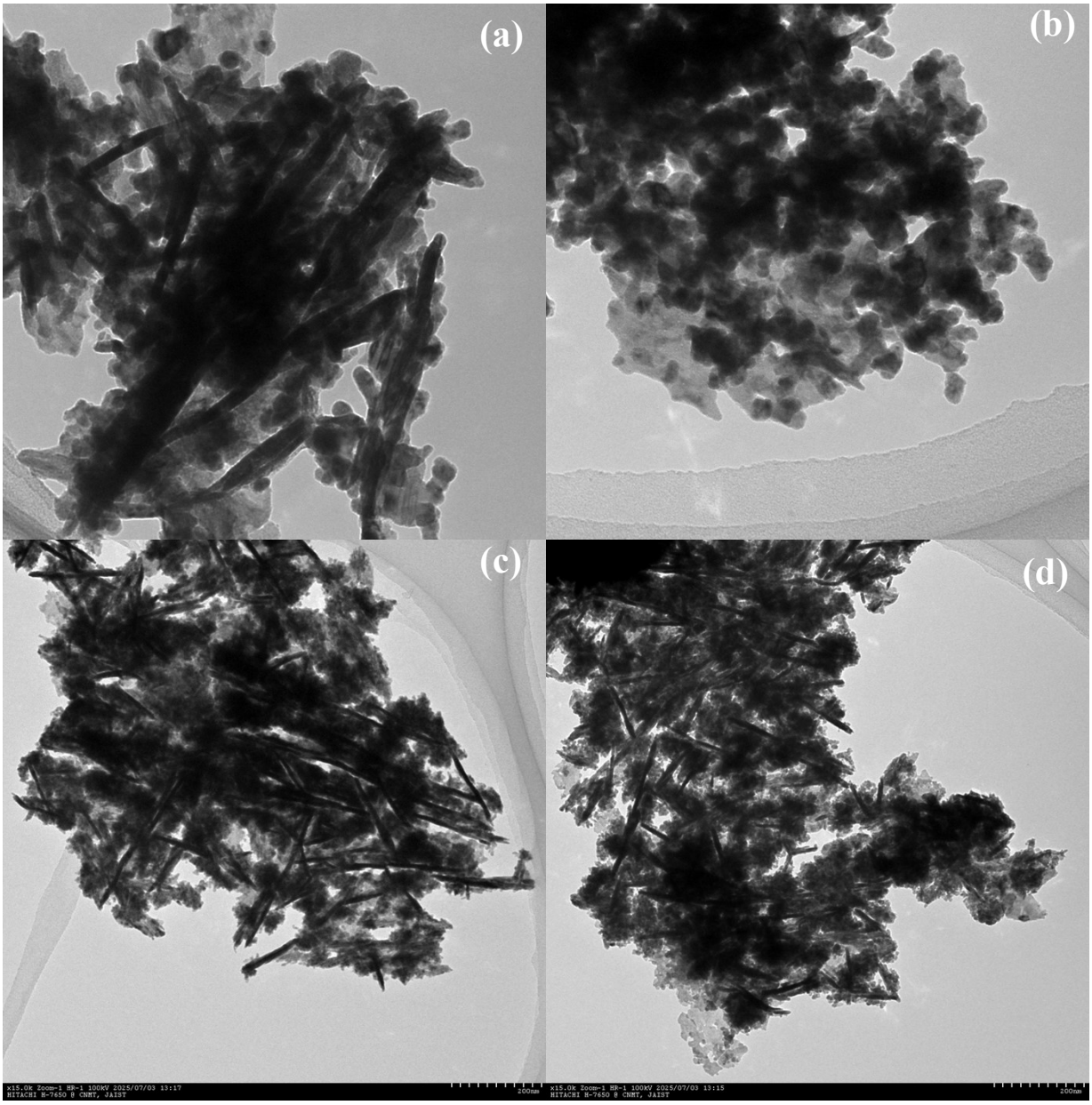
(a)
(b)
(c)
(d)
x15.0k Zoom-1 HR-1 100kV 2025/07/03 13:17
HITACHI H-7650 @ CNMT, JAIST
200nm
x15.0k Zoom-1 HR-1 100kV 2025/07/03 13:15
HITACHI H-7650 @ CNMT, JAIST
200nm

Fig. S5: (a-b) TEM images of Ni-Cuf-3. (c-d) are TEM images of Ni-Cuf-4

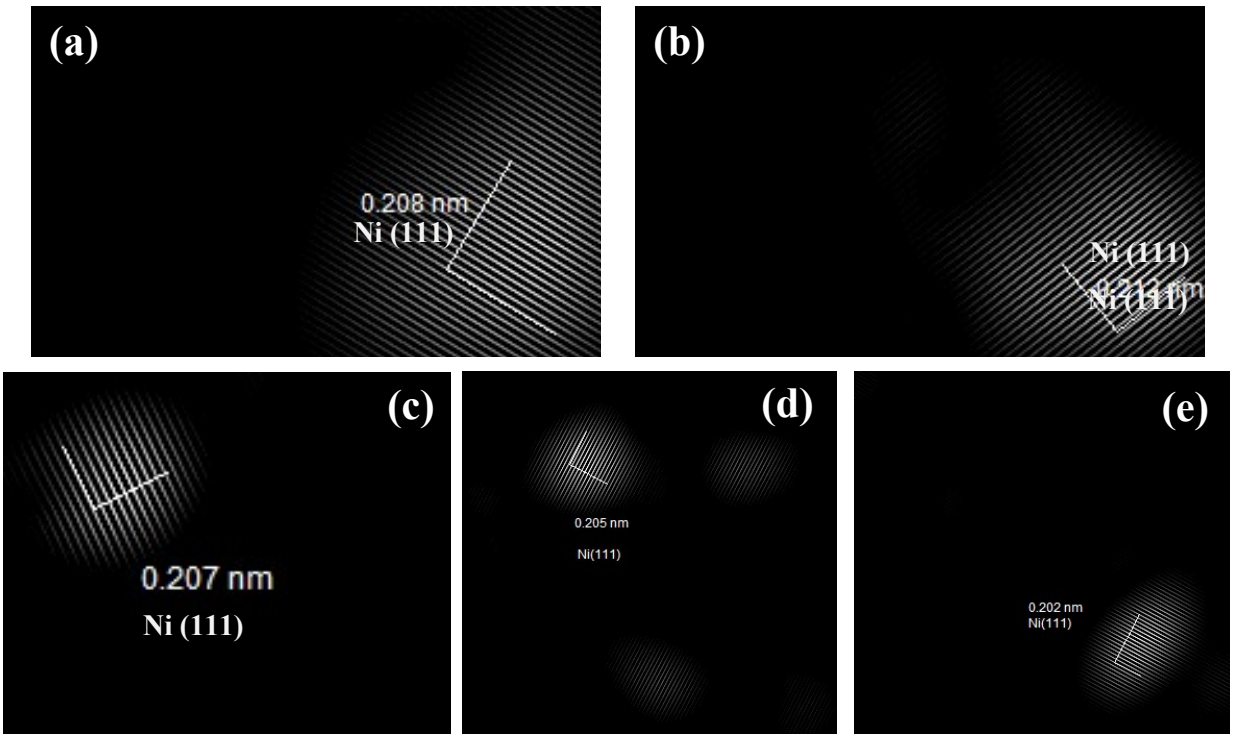

Fig. S6: (a-b) and (c-e) Inverse-FFT images of Ni-Cuf-3 and Ni-Cuf-4 respectively.

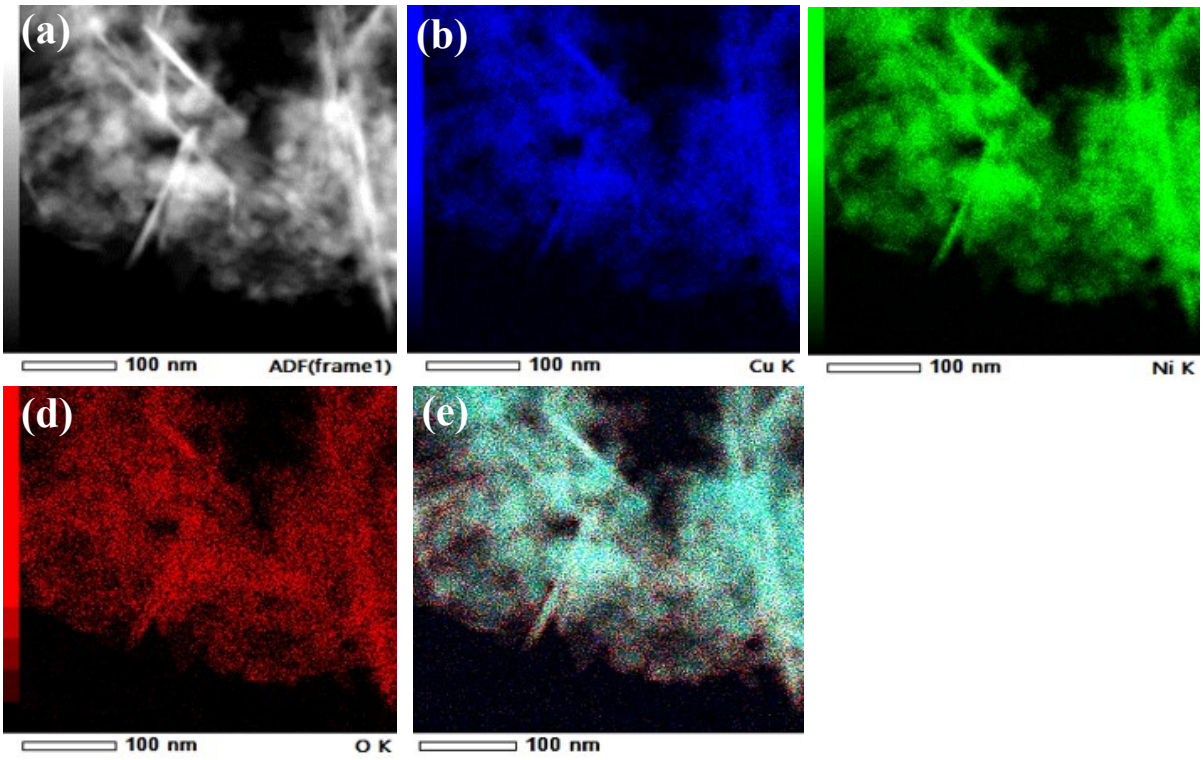

Fig. S7: (a) ADF-STEM image of the analyzed region, (b) Cu K mapping, (c) Ni K mapping, (d) O K mapping, and (e) overlayed elemental map of Ni-Cuf-3

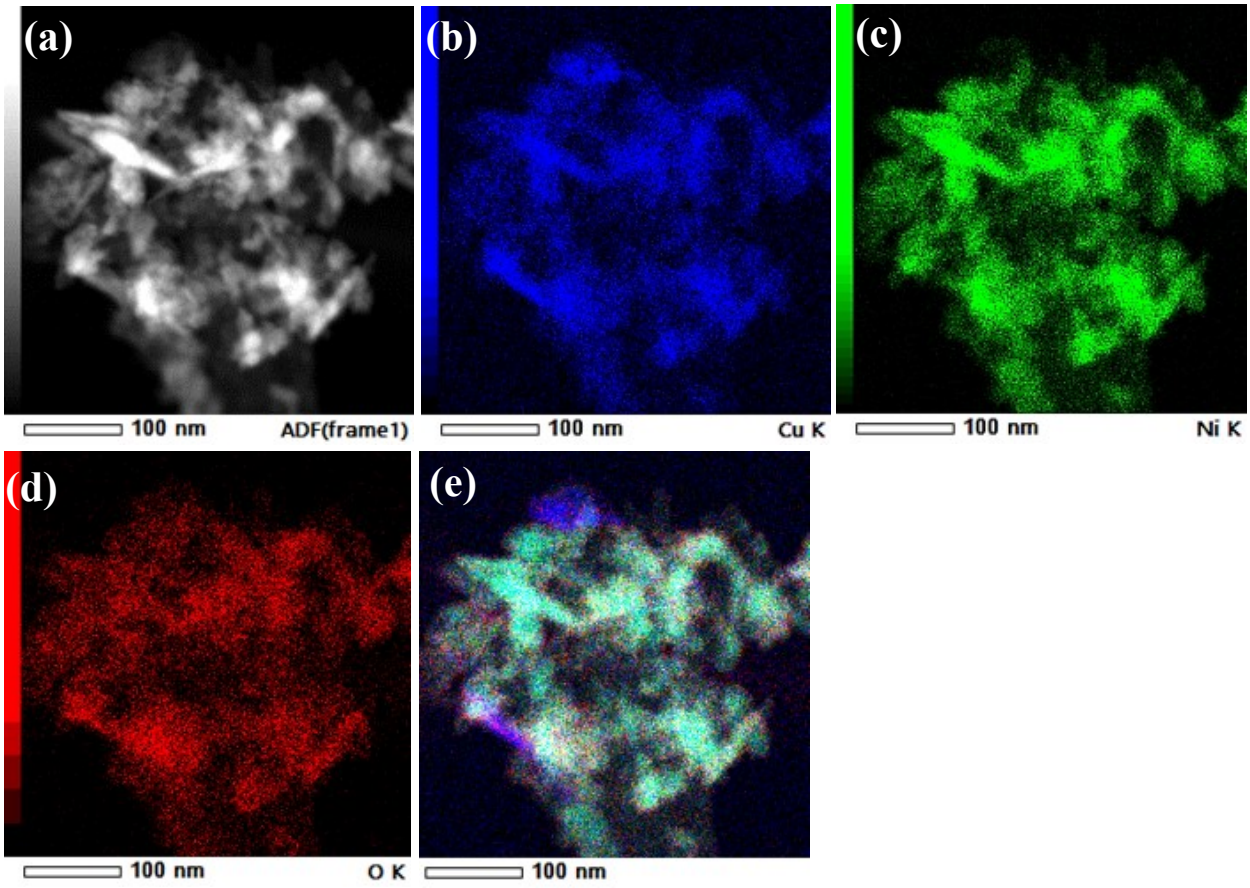

Fig. S8: (a) ADF-STEM image of the analyzed region, (b) Cu K mapping, (c) Ni K mapping, (d) O K mapping, and (e) overlayed elemental map of Ni-Cuf-4

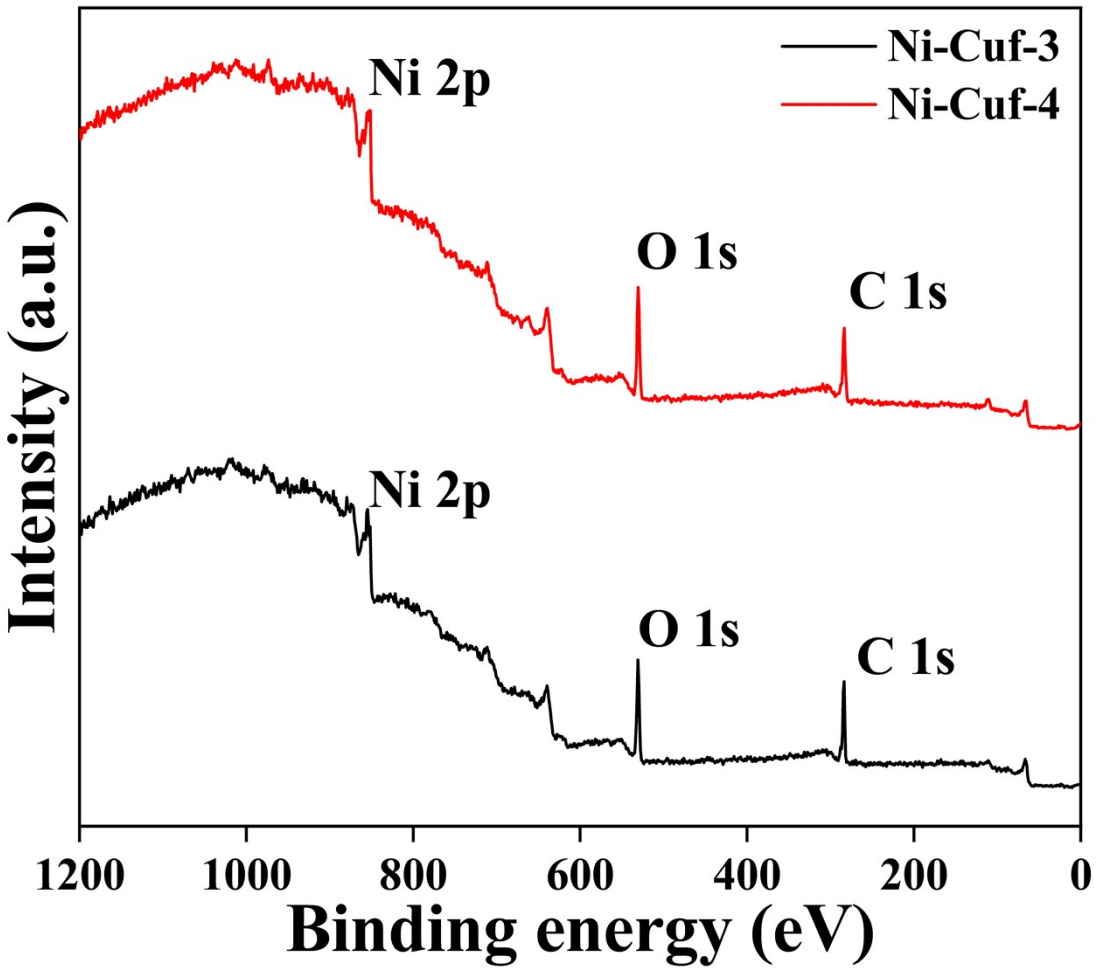

Fig. S9: XPS survey spectra of Ni-Cuf-3 and Ni-Cuf-4

Table S3: EFM amplitude statistical data of Ni-Cuf-3 and Ni-Cuf-4

Electrode	Rpv (mV)	Rq (mV)	Ra (mV)	Rz (mV)	Rsk (mV)	Rku (mV)	Length (μm)
Ni-Cuf-3	4.228	0.824	0.716	2.904	-0.102	2.894	~ 8
	5.346	1.018	0.794	2.801	-0.414	3.577	~ 5
	3.427	0.820	0.695	2.873	0.030	2.087	~10
	3.768	0.870	0.723	3.089	0.818	2.334	~ 8
Ni-Cuf-4	4.736	0.834	0.660	3.670	0.935	4.074	~ 20
	3.138	0.661	0.464	1.358	1.958	6.679	~ 4
	2.138	0.484	0.395	1.686	0.208	2.527	~ 9
	4.386	1.070	0.870	2.850	-0.088	2.407	~ 6
	3.736	0.971	0.792	N/A	0.476	2.461	~ 4
	3.591	0.809	0.683	2.616	0.223	2.247	~ 6

Table S4: EFM quad statistical data of Ni-Cuf-3 and Ni-Cuf-4

Electrodes	Rpv (mV)	Rq (mV)	Ra (mV)	Rz (mV)	Rsk (mV)	Rku (mV)	Length (μm)
Ni-Cuf-3	1.524	0.358	0.288	1.383	0.117	2.447	~9 (H)
Ni-Cuf-4	1.429	0.242	0.192	0.915	-1.010	4.761	~ 8 (V)
	1.105	0.275	0.207	0.895	-1.184	3.695	~ 8 (V)

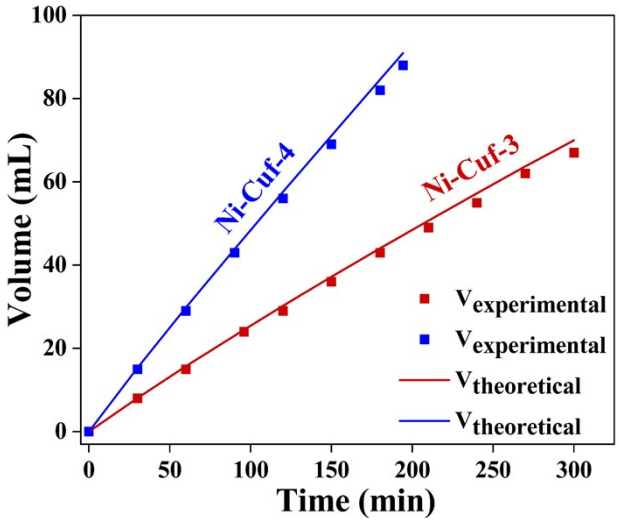

Fig. S10: The amount of theoretically calculated and experimentally measured versus time for OER in 1M KOH. The water displacement setup for O_2 quantification at 2.7 V (Ni foam counter, 2 × 4 cm; ~100 mA cm^{-2}) is shown in ESI† Movie S2.

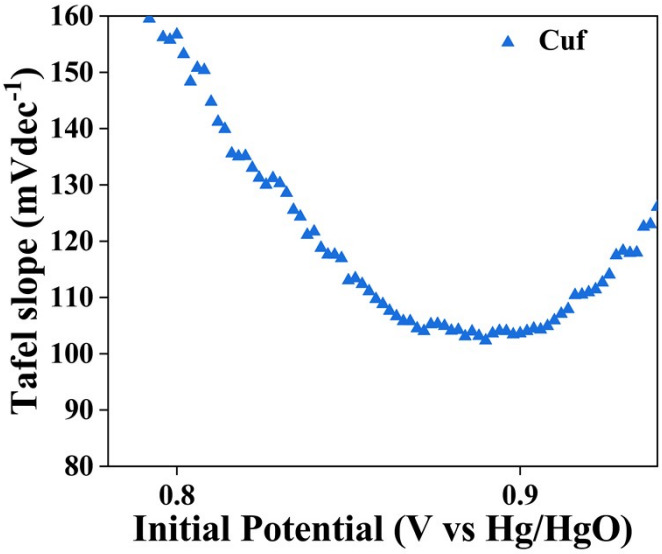

Fig. S11: Tafel slope plot of Cuf

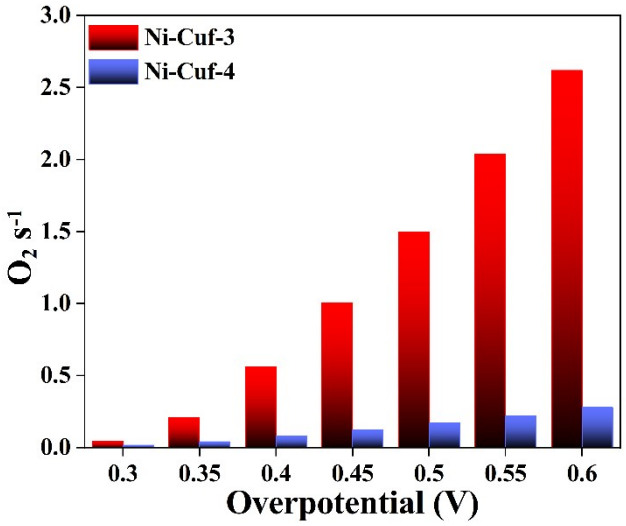

Fig. S12: The turn over frequency (TOF) versus overpotential plot at different overpotentials.

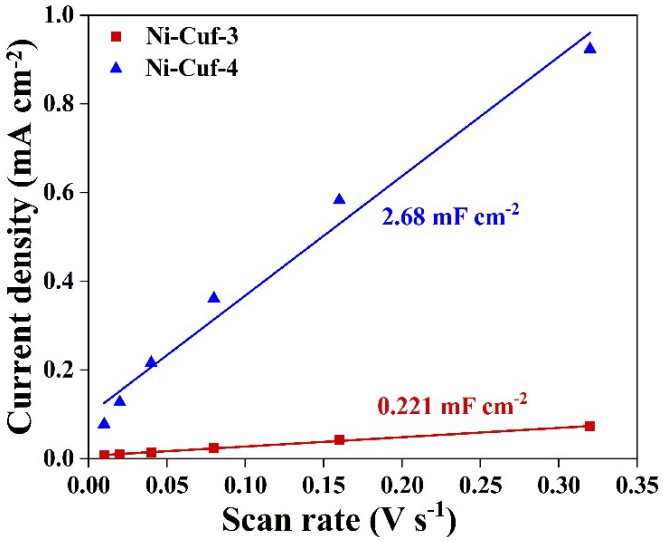

Fig S13: Slope derived from current density plotted against scan rate showing the extraction of the double-layer capacitances

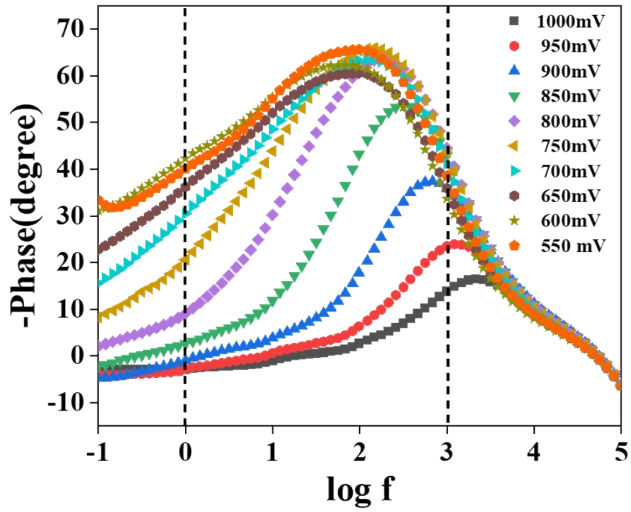

Fig S14: Bode-phase plot of Cuf

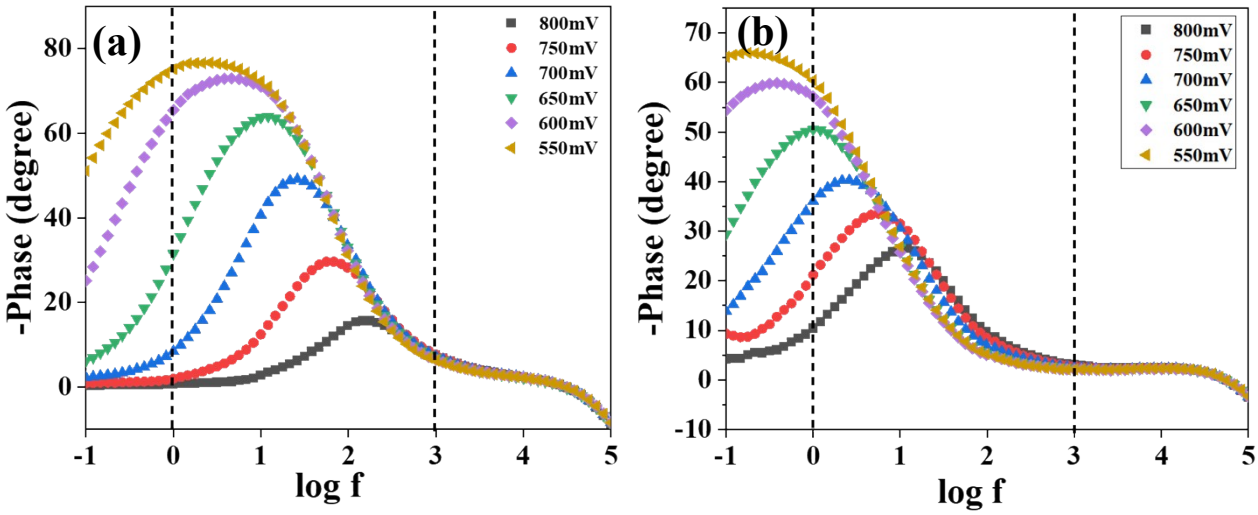

Fig S15: Bode-phase plot of (a) Ni-Cuf-3 and (b) Ni-Cuf-3-after

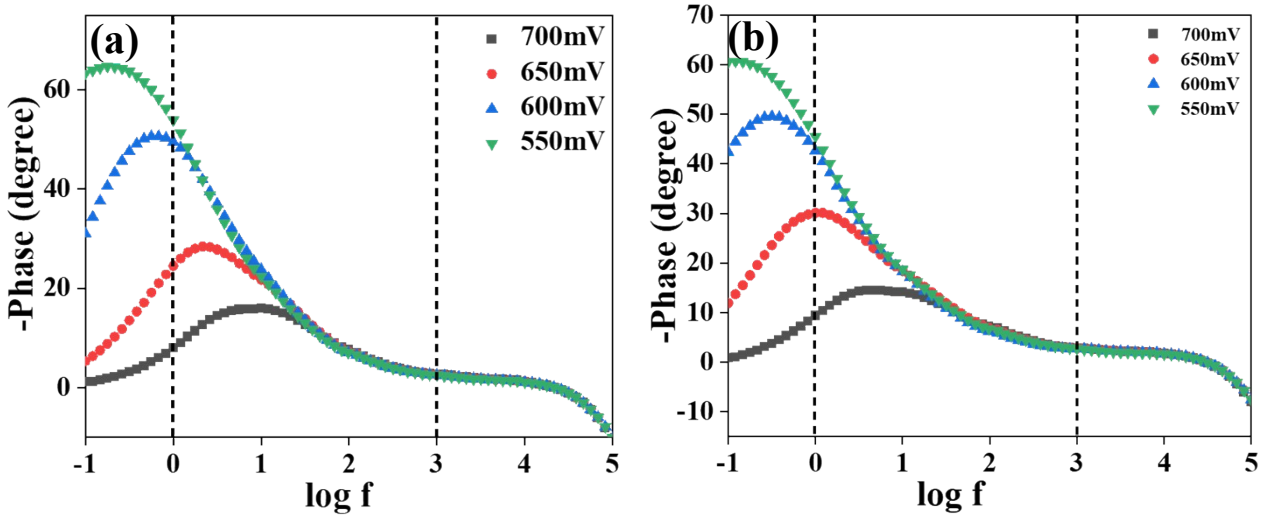

Fig S16: Bode-phase plot of (a) Ni-Cuf-4 and (b) Ni-Cuf-4-after

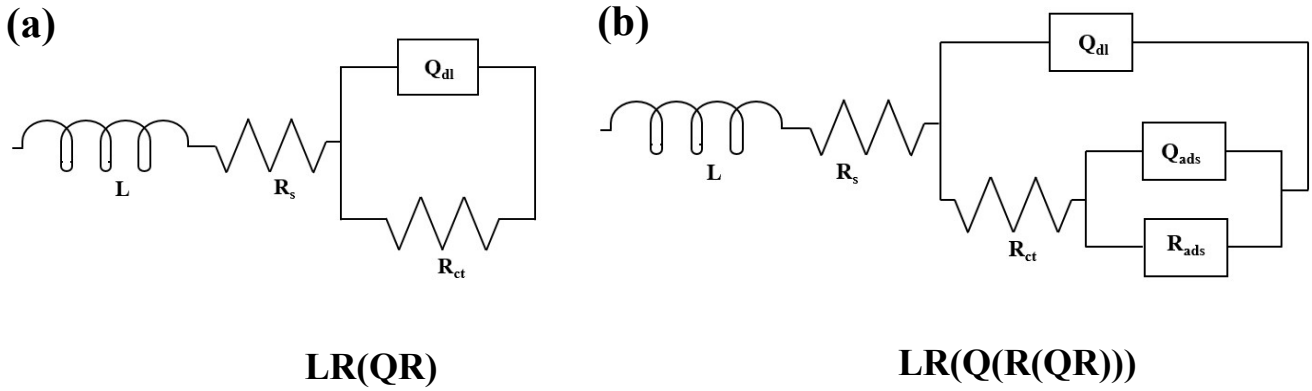

Fig S17: Equivalent Circuit model used EIS fitting

Table S5: R_{ct} values derived by Model fitting using LR(QR) and LR(Q(R(QR))) model.

Potential (V vs Hg/HgO)	LR(QR)					LR(Q(R(QR)))				
	Cuf	Ni-Cuf-3	Ni-Cuf-3-after	Ni-Cuf-4	Ni-Cuf-4-after	Cuf	Ni-Cuf-3	Ni-Cuf-3-after	Ni-Cuf-4	Ni-Cuf-4-after
0.55	582.6	1040	1320	1.65E+11	1040	99.6	952.6	0.5843	0.5515	952.6
0.60	534.2	361	223.6	51.21	168.8	92.56	354.4	210.7	51.22	0.4027
0.65	370.2	74.98	53.01	7.97	12.95	78.74	0.4191	2.077	0.279	0.3734
0.70	308	19.33	23.2	2.976	3.199	77.51	1.93E+01	1.168	2.60E-01	3.31E-01
0.75	206.3	5.556	12.65			93.05	0.3463	12.31		
0.80	93.46	2.038	7.112			70.72	2.098	7.049		
0.85	28.54					1.898				
0.90	8.44					-				
0.95	3.338					2.429				
1.00	1.811				0.6441					

Table S6: R_s values derived by Model fitting using LR(QR) and LR(Q(R(QR))) model.

Potential (V vs Hg/HgO)	LR(QR)					LR(Q(R(QR)))				
	Cuf	Ni-Cuf-3	Ni-Cuf-3-after	Ni-Cuf-4	Ni-Cuf-4-after	Cuf	Ni-Cuf-3	Ni-Cuf-3-after	Ni-Cuf-4	Ni-Cuf-4-after
0.55	1.495	1.912	2.34	1.67	1.912	1.62	1.917	1.946	1.58	1.917
0.60	1.502	1.915	2.332	1.654	1.719	1.611	1.917	2.334	1.654	1.579
0.65	1.493	1.917	2.336	1.636	1.698	1.601	1.787	0.6531	1.527	1.571
0.70	1.492	1.905	2.314	1.617	1.665	1.611	1.906	1.445	1.51	1.545
0.75	1.538	1.879	2.306			1.624	1.762	2.306		
0.80	1.576	1.848	2.293			1.621	9.73E-28	2.30E+00		
0.85	1.601					0.004209				
0.90	1.591									
0.95	1.586					1.609				
1.00	1.592					1.563				

Table S7: C_{dl} values derived by Model fitting using LR(QR) and LR(Q(R(QR))) model.

Potential (V vs Hg/HgO)	LR(QR)					LR(Q(R(QR)))				
	Cuf	Ni-Cuf-3	Ni-Cuf-3-after	Ni-Cuf-4	Ni-Cuf-4-after	Cuf	Ni-Cuf-3	Ni-Cuf-3-after	Ni-Cuf-4	Ni-Cuf-4-after
0.55	7.5190 6E-06	0.0005 3	0.001 34	8.72E -07	0.0005 3	6.3328 4E-05	0.000567	0.00 0102	0.0033 23	0.00 0567
0.60	7.8437 6E-06	0.0005 56	0.002 152	0.002 86	0.0009 58	7.3746 4E-05	0.000572	0.00 2255	0.0028 6	0.00 1238
0.65	7.7545 5E-06	0.0006 07	0.003 097	0.004 232	0.0027 88	2.8910 5E-18	0.000231	1.24 E-11	0.0008 43	0.00 098
0.70	8.8426 6E-06	0.0006	0.002 495	0.004 612	0.0039 65	2.3383 7E-38	0.000605	1.15 E-06	0.0005 99	0.00 0555
0.75	1.5952 8E-05	0.0005 56	0.002 191			0.0001 00776	0.00015	0.00 2209		
0.80	2.5606 1E-05	0.0005 11	0.001 951			0.0001 38451	1.52E-76	0.00 2002		
0.85	3.5369 4E-05					0.0001 43				
0.90	3.9379 5E-05					4.4688 7E-05				
0.95	4.3369 1E-05					6.6259 5E-05				
1.00	4.5337 5E-05					0.0000 9403				

Post-OER analysis of Ni-Cuf-4:

XRD analysis: The redox transformation was accompanied by clear structural changes in XRD patterns (Fig. S18). Low-angle reflections at 14.5° and 18.5° confirmed the formation of hydrated NiOOH phases, with Ni-Cuf-4 showing stronger and broader peaks indicative of increased disorder. Simultaneously, surface oxidation of the copper substrate was evident from diminished Cu(111) intensity and the appearance of new reflections corresponding to Cu_2O and CuO. Importantly, the persistence of metallic Cu(220) confirmed that oxidation remained confined to near-surface regions, without complete loss of metallic Cu in the bulk.

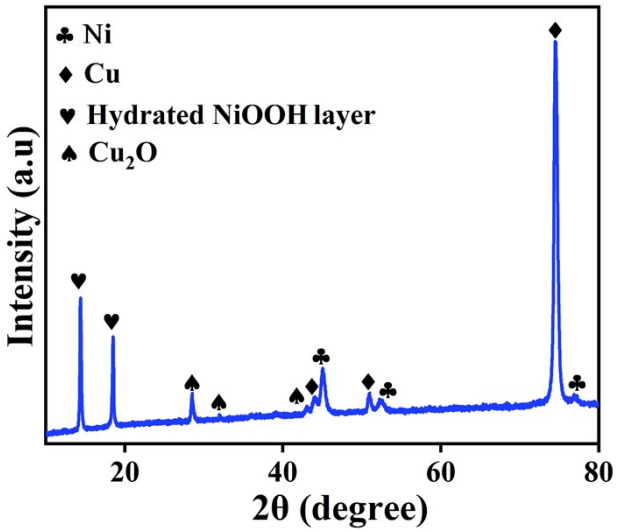

Fig. S18: Post-OER XRD of Ni-Cuf-4 (Ni-Cuf-4-after)

SEM: Following OER, the surface becomes noticeably rougher, with the development of cracks and the emergence of needle-like structures (Fig. S19 (b) and (d)). At higher magnifications, the nodular features appear less distinct, in some cases showing signs of fusion or redeposition. These changes are consistent with surface restructuring under electrochemical stress.

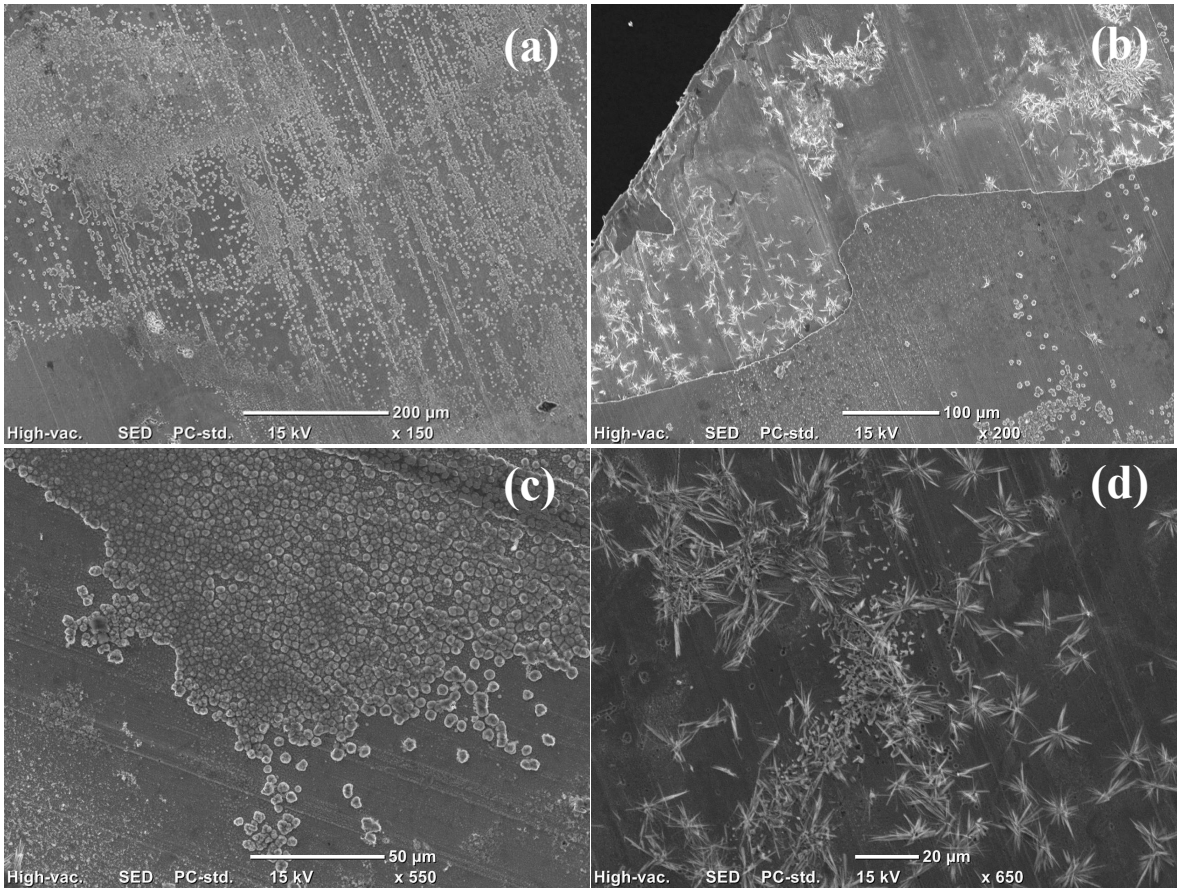

Fig. S19: Post-OER SEM images of Ni-Cuf-4 (Ni-Cuf-4-after)

EDS Mapping: The annular dark-field (ADF) image shows the overall morphology of the Ni-Cuf-4 particle (Fig. S20 (a)). The structure is irregular and porous, consistent with OER-induced surface roughening and hydroxide growth. Copper is mainly concentrated in the inner regions of the particle. This suggests that Cu remains as the underlying structural backbone after OER, consistent with XRD evidence of the persistent metallic Cu(220) phase. Nickel is distributed more broadly across the surface, indicating that Ni remains the dominant surface-active component. The relatively strong and continuous Ni signal suggests that Ni-rich domains stabilize at the electrode–electrolyte interface during OER cycling. Oxygen is homogeneously distributed across the entire particle, reflecting the formation of Ni-O phases (NiOOH/NiO) and partial oxidation of Cu (Cu_2O/CuO). The enrichment of oxygen compared to the pristine state confirms OER-driven oxidation. The merged mapping shows clear overlap of Ni and O signals, verifying the presence of nickel oxyhydroxide phases. Regions with mixed Cu-O signals suggest localized surface oxidation of the Cu substrate. The distribution is

heterogeneous, with metallic Cu-rich domains interspersed with Ni-O-rich regions, consistent with the heterogeneous catalytic interface inferred from electrochemical and XPS data.

EDS mapping confirms that after OER, Ni-Cuf-4 maintains a heterogeneous interface: Cu remains mainly in the bulk/core, while Ni and O dominate the surface, forming NiOOH-rich domains. This supports the electrochemical observation that Ni-Cuf-4 sustains mixed metallic and oxidized regions, enabling both catalytic activity and partial stability despite substrate oxidation.

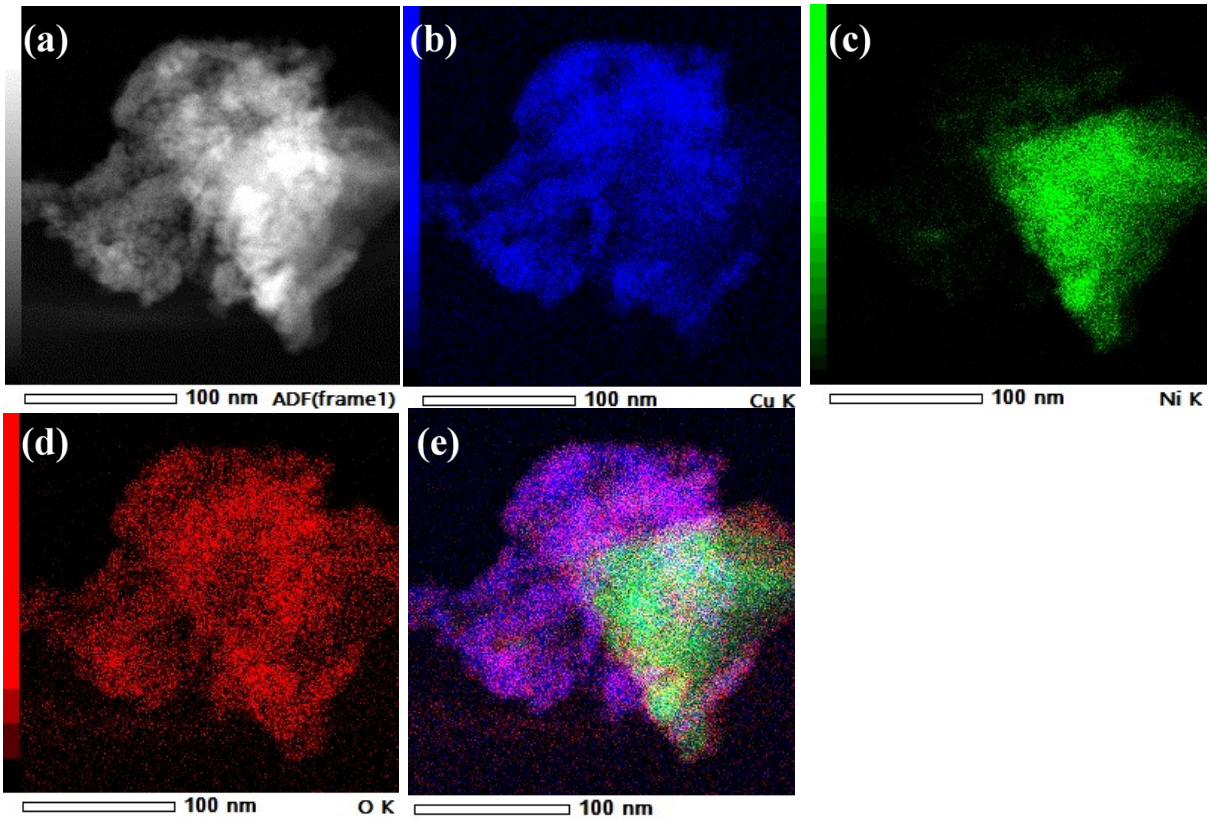

Fig. S20: (a) ADF-STEM image of the analyzed region, (b) Cu K mapping, (c) Ni K mapping, (d) O K mapping, and (e) overlayed elemental map of Ni-Cuf-4-after

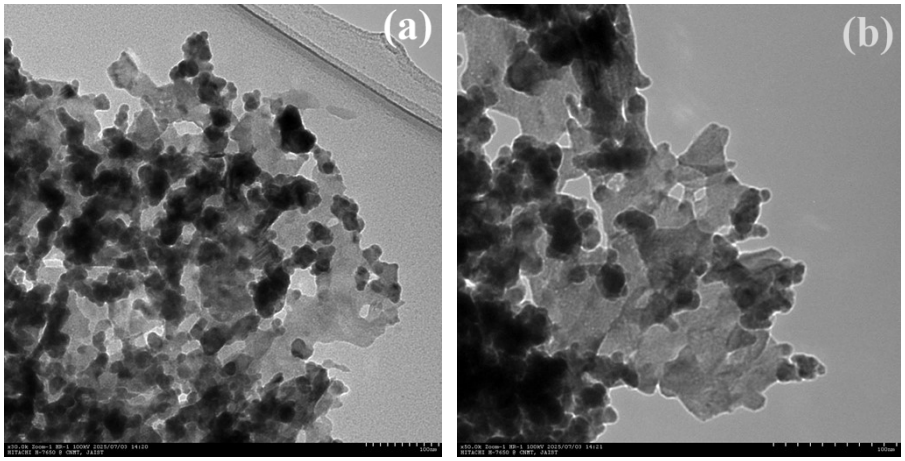

Fig. S21: Post-OER TEM images of Ni-Cuf-4 (Ni-Cuf-4-after)

Overall, the post-OER morphology indicates an increase in surface complexity, which may contribute to greater site exposure but also raises concerns regarding mechanical integrity. The combined evidence suggests a trade-off between the beneficial activation of the electrode and potential degradation effects during prolonged operation.

Table S8. Summary of performance metrics reported in the literature for electrodes fabricated on copper substrates.

Catalyst	Electrolyte	Overpotential (η_{10}) mV	Tafel slope (mV/dec)	Durability	ECSA	RF	Ref
Cu foil	1 M Na_2CO_3 (pH 10.8)	580 (onset = 380 m, ≥ 0.1 mA cm^{-2})	90	NA	-	-	[1]
$Cu(OH)_2$ Nano wire arrays/Cu foil	0.1 M NaOH (pH 12.8)	430 (iR) 530 (Onset at 395 mV)	86	7 h at 4 to 10 $mAcm^{-2}$	49.37 cm^2 (7.9 $mFcm^{-2}$)	197.5	[2]
CuO Nano wire arrays/Cu foil		438 (iR) 530 (onset at 397 mV)	84	-	47.50 cm^2 (7.6 $mFcm^{-2}$)	190.0	
Cu_2O Nano wire arrays/Cu foil		590	-	-	-	-	

CuO_x Nano wire arrays/Cu foil (composite containing both Cu_2O and CuO)		560 (iR) 630 (onset at 440 mV)	108		9.37 cm^2 (1.5 $mFcm^{-2}$)	37.5	
$Cu(OH)_2$ nanowires /Cu foam	1 M KOH	568 @ 100 $mAcm^{-2}$ (onset 400 mV)	89	Significant drop in the current during the initial 2 h of CPE (nanowires peeled off completely from the substrate as witnessed by SEM)	23.3 cm^2	116.5	[3]
CuO nanowires /Cu foam		430 @ 100 $mAcm^{-2}$ (onset 320 mV)	44	180 $mAcm^{-2}$ for 10 h at 1.8 V	31 cm^2	155	
Copper foam		660 @ 100 $mAcm^{-2}$ (onset 470 mV)	159	-	2.5 cm^2	12.5	
Copper foil		750 @ 100 $mAcm^{-2}$ (onset 550 mV)	125	-	0.49 cm^2	2.45	
CuO thin film - nanosheet	1 M KOH	320 530 @ 100 $mAcm^{-2}$ (Onset 300 mV)	135	Significant drop in current after 4h at 20 $mAcm^{-2}$	150 (6 mF cm^{-2})		[4]
CuO thin film - nanocubes		320 550 @ 100 $mAcm^{-2}$ (Onset 280 mV)	149	Significant drop in current after 2h at 20 $mAcm^{-2}$	127.5 (5.1 mF cm^{-2})		

CuO thin film - nanoflowers		270 410 @ 100 $mAcm^{-2}$ (Onset 250 mV)	84	20 $mAcm^{-2}$ for > 14 h at 1.53 V	292.5 (11.7 mF cm^{-2})		
CuO thin film - nanoleaves		280 440 @ 100 $mAcm^{-2}$ (Onset 260 mV)	106	Significant drop in current < 1h at 20 $mAcm^{-2}$	192.5 (7.7 mF cm^{-2})		
Cu2O /Cu plate (LS-Cu-10) (Hierarchical cone-shaped microstructure with porous sponge like nano structures of Cu_2O/Copper plate by femtosecond laser structuring)	1 M KOH	345 (onset 301 mV)	119	9.6 % drop in the current density after 15 h, at 10 $mAcm^{-2}$ 1.53 V	74 cm^2/cm^2 (2.952 $mFcm^{-2}$ from CV) (2.637 $mFcm^{-2}$ from EIS)	61.5	[5]
Cu2O /Cu plate (LS-Cu-20)		380 (onset 335)	121	-	66 cm^2/cm^2 (2.622 $mFcm^{-2}$ from CV) (2.415 $mFcm^{-2}$ from EIS)	54.6	
Cu2O /Cu plate (LS-Cu-50)		412 (Onset 370)	151	-	61 cm^2/cm^2 (2.448 $mFcm^{-2}$ from CV) (2.396 $mFcm^{-2}$	51	

					from EIS)		
Copper plate		587 (Onset 559)	-	-	(0.0271 $mFcm^{-2}$ from CV) (0.0232 $mFcm^{-2}$ from EIS)	0.56	
Petal shaped CuO nano rods, CuO/ $Cu(OH)_2$ /Cu foil	1 M KOH	440	-	> 1h at 10 $mAcm^{-2}$ without any significant reduction in current.	344 cm^2 (13.76 mF cm^{-2})	-	[6]
Petal shaped nanorods $Cu(OH)_2$ /Cu foil		570	-	-	57.75 cm^2 (2.31 mF cm^{-2})	-	
Cu foam	1 M KOH	447 mV (iR) @ 20 mA cm^{-2}	143	-	3.7 mF cm^{-2}	-	[7]
Ni-Mo/ Cu foam		316 mV (iR) @ 20 mA cm^{-2}	70	-	4.1 mF cm^{-2}	-	
Cu nanowires/ Cu foam		372 mV (iR) @ 20 mA cm^{-2}	92	-	81.25 mF cm^{-2}	-	
Ni/Cu nanowires/ Cu foam		-	97	-	42.6 mF cm^{-2}	-	
Mo/Cu nanowires/ Cu foam			99	-	50.3 mF cm^{-2}	-	
Ni-Mo/Cu nanowires/ Cu foam		280 mV (iR) @ 20 mA cm^{-2}	66	12 h	90.7 mF cm^{-2}	-	
Ni / Cu foil	1 M KOH	(Onset 170 mV)	85	~ 2.2 h @ 1.45 V	0.61 cm^2	-	[8]
Ni-ITO nano		(Onset 140 mV)	73	~ 2.2 h @	1.84 cm^2	-	

composite / Cu foil				1.45 V			
Cu	0.1 M KOH	-	170	-	-	-	[9]
Cu/Ni		230 mV @ 5 mA cm^{-2}	126	-	-	-	
Cu/Ni/MoO_3		140 mV @ 5 mA cm^{-2}	73	-	-	-	

References:

1. J. Du, Z. Chen, S. Ye, B. J. Wiley and T. J. Meyer, Copper as a Robust and Transparent Electrocatalyst for Water Oxidation, 2015, **54**, 2073-2078.

2. C.-C. Hou, W.-F. Fu and Y. Chen, Self-Supported Cu-Based Nanowire Arrays as Noble-Metal-Free Electrocatalysts for Oxygen Evolution, 2016, **9**, 2069-2073.

3. C. Lu, J. Wang, S. Czioska, H. Dong and Z. Chen, Hierarchically Structured Cu-Based Electrocatalysts with Nanowires Array for Water Splitting, *The Journal of Physical Chemistry C*, 2017, **121**, 25875-25881.

4. F. Arshad, A. Munir, Q. Q. Kashif, T. u. Haq, J. Iqbal, F. Sher and I. Hussain, Controlled development of higher-dimensional nanostructured copper oxide thin films as binder free electrocatalysts for oxygen evolution reaction, *International Journal of Hydrogen Energy*, 2020, **45**, 16583-16590.

5. S. Ahmad, M. Egilmez, A. M. Kannan and A. S. Alnaser, Oxygen evolution reaction enhancement of copper electrodes in alkaline medium using ultrafast femtosecond laser structuring, *International Journal of Hydrogen Energy*, 2024, **52**, 2-13.

6. C. Xie, K. Zhang, Y. Lai, L. Du, J. Ma, S. Xu and P. Qiu, Elucidating the Mechanism of Oxygen Evolution Reaction on Nanostructured Copper-Based Catalysts, *ACS Applied Nano Materials*, 2024, **7**, 2033-2040.

7. S. Zhao, J. Huang, Y. Liu, J. Shen, H. Wang, X. Yang, Y. Zhu and C. Li, Multimetallic Ni–Mo/Cu nanowires as nonprecious and efficient full water splitting catalyst, *Journal of Materials Chemistry A*, 2017, **5**, 4207-4214.

8. P. Sivasakthi, M. V. Sangaranarayanan and H. Gurumallesh Prabu, Micro–nanoarchitectures of electrodeposited Ni–ITO nanocomposites on copper foil as electrocatalysts for the oxygen evolution reaction, *New Journal of Chemistry*, 2021, **45**, 5146-5153.

9. P. K. R. Kuppam, K. M. M. D. K. Kimbulapitiya, S. Vuppala, K. Wang, G. P. Reddy, K. P. Pande, P.-T. Lee and Y.-L. Chueh, A Nickel Coated Copper Substrate as a Hydrogen Evolution Catalyst, 2022, **12**, 58.